Eur. Phys. J. B **12**, 241–251 (1999)

THE EUROPEAN PHYSICAL JOURNAL B

EDP Sciences

A Monte-Carlo study of equilibrium polymers in a shear flow

A. Milchev[1,a], J.P. Wittmer[2,b], and D.P. Landau[3]

[1] Institute for Physical Chemistry, Bulgarian Academy of Sciences, 1113 Sofia, Bulgaria
[2] Département de Physique des Matériaux, Université Claude Bernard Lyon I, 69622 Villeurbanne Cedex, France
[3] Department of Physics and Astronomy, University of Georgia, Athens, Ga. 30602, USA

Received 22 October 1998 and Received in final form 12 April 1999

Abstract. We use an off-lattice microscopic model for solutions of equilibrium polymers (EP) in a lamellar shear flow generated by means of a self-consistent external field between parallel hard walls. The individual conformations of the chains are found to elongate in flow direction and shrink perpendicular to it while the average polymer length decreases with increasing shear rate. The Molecular Weight Distribution of the chain lengths retains largely its exponential form in dense solutions whereas in dilute solutions it changes from a power-exponential Schwartz distribution to a purely exponential one upon an increase of the shear rate. With growing shear rate the system becomes increasingly inhomogeneous so that a characteristic variation of the total monomer density, the diffusion coefficient, and the center-of-mass distribution of polymer chains of different contour length with the velocity of flow is observed. At *higher* temperature, as the average chain length decreases significantly, the system is shown to undergo an order-disorder transition into a state of nematic liquid crystalline order with an easy direction parallel to the hard walls. The influence of shear flow on this state is briefly examined.

PACS. 83.50.Ax Steady shear flows – 82.35.+t Polymer reactions and polymerization – 61.25.Hq Macromolecular and polymer solutions; polymer melts; swelling – 64.60.Cn Order disorder transformations; statistical mechanics of model systems

1 Introduction

Systems in which polymerization takes place under condition of chemical equilibrium between polymer chains and their respective monomers are termed "equilibrium polymers" (EP) [1]. The interest to EP from the point of view of both applications and basic research has recently triggered numerous investigation, including computer simulations [4,5] in an effort to avoid difficulties with laboratory experiments [6] and approximations as the Mean Field Approximation (MFA). Recently the basic scaling concepts of polymer physics were tested by extensive Monte-Carlo (MC) simulations of flexible EP on a lattice [4]. The results suggest that despite polydispersity, EP resemble conventional polymers (where the polymerization reaction has been deliberately terminated) in many aspects. However, dynamic aspects of their behavior may still be very different: for example, the constant process of scission and recombination in EP offers an additional mechanism of stress relaxation [7]. Computer experiments on EP dynamics are already under way [8].

Considerably fewer simulation studies of *non-equilibrium* properties of EP have been reported [5,9]. Recently observed phenomena such as shear banding structure, shear inducing structure and phase transitions [12–15] are not completely understood. An earlier theoretical work [16], for instance, predicted a decrease in average size of dilute rod-like micelles whereas a later study [17] concluded that rod-like micelles should grow at higher shear rates. Since it is known that viscoelastic surfactant solutions show unusual nonlinear rheology [18], it is clear that much more research in this field is needed before complete understanding of rheological properties of EP is achieved.

Since EP behave in many respects as conventional "dead" polymers [4], comparisons with the latter where much more work on shear flow effects has been done so far, could prove very useful. Thus inhomogeneity of flows, due to the presence of boundaries, and its impact on polymer behavior may be directly observed experimentally by means of evanescent wave-induced fluorescence method [19] that can probe the polymer concentration in the depletion layer adjacent to the walls. Coil stretching of dilute flexible polymers in a flow, diffusion and density profiles as well as "slip" effects near walls have been treated theoretically [20–23] and by computer simulations [24–26], and as we shall demonstrate below, many of these early results compare favorably with what we observe for EP in the present investigation.

[a] e-mail: milchev@ipchp.ipc.bas.bg
[b] e-mail: j.wittmer@dpm.univ-lyon1.fr

In the present study we employ a dynamic Monte-Carlo algorithm in order to study EP properties in shear rate. The flow of the system in a semi-infinite slit of thickness D is induced by applying an external field F with magnitude which changes linearly across the slit and is parallel to the hard walls of the container. Thus the jump rate of the monomers becomes biased along the x-axis and a flow of the system through the periodic boundary sets in.

One should emphasize that such an investigation should focus on the linear response in a laminar shear flow. MC methods cannot account for hydrodynamic interactions in principle and the transition from laminar to turbulent flow can be simulated by means of Molecular Dynamics (MD) only. The linear response breaks down at field intensities when the maximum flow velocity is attained, *i.e.* when all 100% of the random jumps along the x-axis are forced to occur, say, in positive direction. Any further increase of the field F will then fail to accelerate the particles any further. Even with these limitations, however, it appears that this kind of MC simulation of EP in a shear flow is warranted, given the considerably longer time periods or systems sizes a MC methods may handle as compared to MD.

All Monte-Carlo studies of EP so far have been performed on a cubic lattice either exploiting an analogy of the Potts model of magnetism to random self-avoiding walks on a lattice [10,11], or using the Bond Fluctuation (BFL) Model [4,9]. These lattice models were developed and extensively used for monodisperse systems of conventional polymers and are known to faithfully reproduce their dynamic (Rouse) behavior. For the purpose of shear flow studies a disadvantage of these models, due to the discrete structure of the lattice, appears obvious: monomers would block each other on the lattice at higher shear rates. Random jumps would have to be of the size of single monomers only, and, last not least, the artificial cubic symmetry would predetermine ordering effects along the three major axes of the lattice [27] thereby questioning possible phase transitions into liquid crystalline order.

In the present work we employ an off-lattice model of EP, designed to overcome these and other shortcomings of previous lattice models and to serve in examining the role of polymers (semi)-flexibility. An off-lattice model should be a better tool in dynamic studies of a broader class of soft condensed matter systems where bifunctionality of the chemical bonds might be extended to polyfunctional bonds, as this is the case in gels and membranes. A comprehensive comparison of this off-lattice algorithm to earlier lattice models [8] shows that all properties of EP derived in former investigations, are faithfully reproduced in the continuum too.

2 Description of the model

As in our earlier off-lattice bead-spring model of conventional polymer chain [28,29], a coarse-grained polymer chain consists of l beads or "effective monomers". These are connected by springs which represent "effective bonds" and are described by a FENE (finitely extendible nonlinear elastic) potential:

$$U_{\rm FENE}(r) = -\frac{k}{2}R^2 \log\left[1-\left(\frac{r-r_0}{R}\right)^2\right] - J, \quad (1)$$
$$\text{for } -R < r - r_0 < R,$$
$$U_{\rm FENE}(r) = \infty, \text{ otherwise}$$

where r is the distance between two successive beads, $r_0 = 0.7$ is the unperturbed bond length with maximal extension $l_{\max}$, $R = l_{\max} - r_0 = 0.3$, and $k/2 = 20$ (in our units of energy $k_{\rm B}T = 1.0$) is the elastic constant of the FENE potential which behaves as a harmonic potential for $r - r_0 \ll R$. Thus $U_{\rm FENE}(r \approx r_0) \approx -\frac{k}{2}(r-r_0)^2$ but diverges logarithmically both for $r \to l_{\max}$ and $r \to l_{\min} = 2r_0 - l_{\max}$. We choose our unit of length such that $l_{\max} = 1$ and then the hard core diameter of the beads $l_{\min} = 0.4$. All lengths as, *e.g.* the linear size of the simulational box, are then measured in units of $l_{\max}$.

According to equation (1) the net gain of energy of a monomer which forms a bond with a nearest neighbor at distance r_0 is then equal to the "bond" energy J. In EP these strong attractive bonds between nearest neighbors along the backbone of a chain are constantly subject to scission and recombination. In the present model only bonds, stretched a distance r beyond some threshold value, $r_{\rm break} = 0.8 l_{\max}$, attempt to break so that eventually an energy $U_{\rm FENE}(r) > 0$ in the interval between 0 and J could be released if the bond is broken.

Each monomer has two unsaturated bonds which may be either engaged in forming a strong saturated bond between nearest neighbors along the backbone of a chain (when the originally unsaturated bonds of such neighbors meet and become a parallel pair) or remain free (or "dangling") as in the case of chain ends or non-bonded single monomers. In order to create a bond, however, the respective monomers must approach [1] each other within the same interval of distances $r_{\rm break} \le r \le l_{\max}$ where scissions take place. While covalent bonds are thus constantly broken or created during the simulation, we would like to emphasize that no formation of ring polymers is allowed and this condition has to be observed whenever an act of polymerization takes place.

The non-bonded interaction between monomers is described by a Morse potential,

$$U_{\rm M}(r) = \exp\left[-2a\left(r - r_{\min}\right)\right] - 2\exp\left[-a\left(r - r_{\min}\right)\right],$$
$$\text{for} \quad 0 < r - r_{\min} < \infty, \quad (2)$$

where $r_{\min} = 0.8$, and the large value of $a = 24$ makes interactions vanish at distances larger than unity, so that an efficient *link-cell* algorithm [28] for short-range interactions can be implemented. In the present study we maintain our system in the "good solvent" regime and, therefore, only keep the repulsive branch of equation (2), shifting it up the positive y-axis so that $U_{\rm M}(r) = 0$ for

[1] Recombination for $r < r_{\rm break}$ would violate detailed balance if scissions occur at $r > r_{\rm break}$ only.

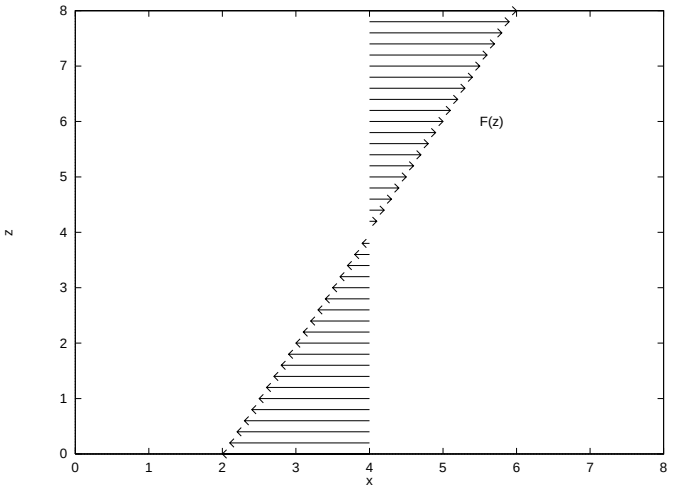

Fig. 1. Definition sketch for external field variation, $F_x(z)$, causing flow in x-direction between infinite parallel plates.

$r > r_{\min}$. The radii of the beads and the interactions, equations (1, 2), have been chosen such that the chains may not intersect themselves or each other in the course of their movement within the box, so that "excluded-volume" interactions as well as the topological connectivity of the macromolecules are allowed for.

We introduce the shear rate B by defining an external field $\mathbf{F}$ whose only component is directed along the x-axis and changes linearly along the z-dimension of the box – Figure 1:

$$F_x(z) = B(z - Z_{\max}/2), \quad \frac{\mathrm{d}F_x(z)}{\mathrm{d}z} = B \tag{3}$$

so that the bias changes sign at the middle of the box $Z_{\max}/2$.

A standard Metropolis algorithm governs monomer displacements, whereby an attempted move of a randomly selected particle in a random direction is taken from a uniform distribution within the interval $-\frac{1}{2} \leq \Delta x, \Delta y, \Delta z \leq \frac{1}{2}$. The presence of impenetrable walls at $z = 0$ and $z = Z_{\max}$ is observed by rejection of all those jumps of the monomers which would otherwise cause them to leave the box through the planes at the bottom and the top. Thus jumps are attempted with probability

$$P_{\mathrm{att}}(\Delta x) = \begin{cases} 1, & \text{for} \quad -\frac{1}{2} \leq \Delta x \leq \frac{1}{2} \\ 0, & \text{otherwise} \end{cases} \tag{4}$$

and *accepted* with probability, equal to

$$P_{\mathrm{acc}}(\Delta x) = \exp[-(E_{\mathrm{new}} + \Delta W - E_{\mathrm{old}})/k_{\mathrm{B}}T], \quad \text{for} \quad E_{\mathrm{new}} + \Delta W > E_{\mathrm{old}},$$

$$P_{\mathrm{acc}}(\Delta x) = 1 \quad \text{otherwise}, \tag{5}$$

where E_{new} and E_{old} are the energies of the new and old system configurations, and ΔW is the work, performed by the field when a monomer jumps from position $\mathbf{r}_{\mathrm{old}}$ to a new position, $\mathbf{r}_{\mathrm{new}}$:

$$\Delta W = \int_{\mathbf{r}_{\mathrm{old}}}^{\mathbf{r}_{\mathrm{new}}} \mathbf{F}\mathrm{d}\mathbf{r} = \int_0^{\Delta x} F(z(x))\mathrm{d}x. \tag{6}$$

Since the potential of the field $\mathbf{F}$, equation (3), is not scalar, ΔW depends on the path followed by the monomer during a jump $\mathbf{r}_{\mathrm{old}} \rightarrow \mathbf{r}_{\mathrm{new}}$. During a jump this path $z(x)$ is a straight line, $z(x) = \frac{\Delta z}{\Delta x}x + z_{\mathrm{old}}$, so that from equation (3) one obtains for the work

$$\Delta W = \int_0^{\Delta x} F_x \mathrm{d}x = B\frac{z_{\mathrm{new}} + z_{\mathrm{old}}}{2}\Delta x = \bar{F}\Delta x, \tag{7}$$

where $\bar{F}$ denotes the *average* from the values of the field in positions $\mathbf{r}_{\mathrm{old}}$ and $\mathbf{r}_{\mathrm{new}}$. With $\bar{F}$, as defined in equation (7), one satisfies the condition of *microscopic reversibility* with respect to the movements of the particles. Note that it is the microscopic reversibility which requires the use of $\bar{F}$, rather than F_{old}, for instance, in the determination of ΔW. This becomes immediately obvious by considering the displacement of a single non-interacting particle in the external field: for a self-consistent algorithm, the update rules for the forward and reverse moves have to be identical (time reversible).

The field, $\mathbf{F}$, is thus introduced in the system as an additional term in the Boltzmann probability in equation (5) whereby the probability for jumps along or against the field becomes then strongly biased. This term makes the energy in the Boltzmann factor in equation (5) a monotonously decreasing function of x. The Metropolis algorithm tends to find the minimum of this energy thus continuously driving the system to an unreached minimum which gives a continuous flow in x direction. One can readily estimate the average jump distance, δx, if ΔW is assumed to be larger than the microscopic interactions U_{FENE} and U_{M}. Setting $E_{\mathrm{new}} \approx E_{\mathrm{old}} = 0$ for simplicity in equation (5), with $\bar{F} \approx F$ one has

$$\delta x = \frac{\int x P_{\mathrm{acc}}(x)\mathrm{d}x}{\int P_{\mathrm{acc}}(x)\mathrm{d}x} = \frac{\int_0^{\frac{1}{2}} x\exp(-Fx)\mathrm{d}x + \int_{-\frac{1}{2}}^0 x\mathrm{d}x}{\int_0^{\frac{1}{2}} \exp(-Fx)\mathrm{d}x + \int_{-\frac{1}{2}}^0 \mathrm{d}x} = \frac{-\frac{1}{8} + [1 - (1 + \frac{F}{2})\exp(-\frac{F}{2})]/F^2}{\frac{1}{2} + [1 - \exp(-\frac{F}{2})]/F} \tag{8}$$

which yields $\delta x = 0$ for $F = 0$ and $\delta x \approx -\frac{1}{4}$ for sufficiently strong fields F, (the sign of δx depending on which half of the box is considered). Thus δx remains bound from above, no matter how strong the applied bias is chosen[2].

In order to provide for the reversibility of scission and recombination events, a Monte-Carlo time step (MCS) has been performed after N particles of the system are randomly chosen and attempted to move at random whereby existing bonds are kept as they are. After that N monomers are again picked at random, *i.e.* one

[2] Of course, since the microscopic interactions are always present, this result remains a rough estimate only whose validity can be checked by the simulation.

of the two bonds of each is randomly chosen and, depending on whether this bond exists and points to an existing neighbor along the same chain, or it doesn't, the bond is attempted to break or to create.

Thus, within an elementary time step (MCS) N random jumps and as many attempts of bond scission/recombination are carried out, each subject to the Boltzmann probability that the respective attempt is successful. It is clear that in a system of EP where scission and recombination of bonds are constantly taking place the particular scheme of bookkeeping is no trivial matter. Since the identity of a particular chain, or monomer affiliation, is in principle preserved for no more than one MCS, the data structure of the chains can only be based on the individual monomers (or, rather, links) as suggested recently [4]. Thus each monomer has two links. The links associated with a given monomer are pointers which may either point to another link or to "nowhere". In the latter case a link then represents an unsaturated dangling bond. Thus a large number of particles may be simulated at very modest operational memory. Results in the present study involve systems of up to $N = 65536$. The simulational box (slit) sizes are typically $16 \times 16 \times D$ where D is the width of the slit in z-dimension. The total density of the monomers c is then defined as the number of monomers per unit volume.

During the simulation the whole system is periodically examined, the number of chains with chain length l, square end-to-end distance, R_e^2, gyration radius, R_g^2, center-of-mass coordinates, displacements, etc., are counted and stored. Because of the semi-periodic (in x- and y-direction) boundary conditions the interactions between monomers follow the minimum image convention. The computation of the conformational properties of the chains as R_e^2, for instance, then implies a restoration of the *absolute* monomer coordinates from the periodic ones for each repeating unit of the chain.

Technical details of this new algorithm will be presented elsewhere, here we will note only that the high efficiency in code performance is achieved by extensive implementation of integer arithmetic in this off-lattice model based largely on binary operations with variables. Thus, for example, the most heavily involved (modulo) operations which provide periodicity of coordinates and the minimum image computation for distances turn out to be redundant.

3 Simulational results

3.1 Velocity profiles

As mentioned in Section 2, we create a shear flow in our system by applying an external field with constant gradient along the z-axis of the box so that the flow is oriented along the x-direction – *cf.* equation (5), parallel to the hard walls at $z = 0$ and $z = D$. The lower half of the box would then flow in positive, the upper one – in negative x-direction. It is expected that in the immediate vicinity of the walls the flow might be somewhat distorted due to walls impenetrability. Below, in Figure 2a we plot the mean jump distance per MCS, δx, measured along the x-axis for different values of B. The z-coordinates of these successful jumps are taken from the respective z-coordinate of the monomers.

Evidently, in a wide channel with $D = 32$ only for sufficiently weak field $B \leq 0.3$ the average jump distance grows linearly with respect to the half-width of the box (for $B = 0$ it is zero). For $B > 0.3$ distortions in the δx profile set in because the maximal jump distance is limited to 0.5, as mentioned in Section 2. For a more narrow slit of width $D = 16$ the region of linear response would then extend to higher values of $F \leq 0.7$. Therefore most of the simulational results in what follows are derived for $D = 16$. Figure 2b then demonstrates that the velocity changes linearly across the slit for sufficiently small values of the field B.

In the broad channel, $D = 32$, at $z = 0, D$ for $B = 0.5$ one gets $F = 8$ from equation (3) so that the average jump distance there according to equation (8) should be $\delta x \approx \pm\, 0.178$. The value of δx at the borders of the box, as seen from Figure 2a, confirms this estimate demonstrating that the role of the microscopic interactions U_{M} and U_{FENE} is small.

The presence of the walls is felt in their immediate vicinity and some local distortion of the displacement profile appears increasingly pronounced with growing B although it remains spatially contained in a layer of thickness roughly equal to monomers diameter. It is interesting to note that this small increase of δx (and, therefore, of velocity) immediately at the walls resembles the so called "slip effect" [23,24] in simple shear flow of dilute polymer solutions in a narrow channel. This slip effect can be explained intuitively by the fact that the polymer molecules near the wall align themselves more strongly with the flow than those away from the wall, and are thus transporting less flow-wise momentum across the flow than would otherwise be the case. Indeed, in our Monte-Carlo model the attempted jumps which would otherwise bring the monomers through and beyond the walls of the slit are always rejected. Since the molecules cannot penetrate the wall, their concentration is reduced at the wall, so that their contribution to the viscosity is further diminished. Using a model of dumbbells in parallel wall shear flow, one can calculate [21,23,24] both the nonlinear velocity profile of the suspended solutions as well as the center of mass concentration profile between the two walls – we shall see in the next section that the latter is qualitatively reproduced by our simulational results.

3.2 Effect of shear rate on average chain length and molecular weight distribution

We find that the average chain length of the EP solution, L, decreases steadily with growing B, which is in agreement with an earlier MD study [5] – Figure 3: the mean chain length L at this highest shear rate is about 70% of its value for a system at rest. Here we should like to point out the existence of considerable fluctuations in

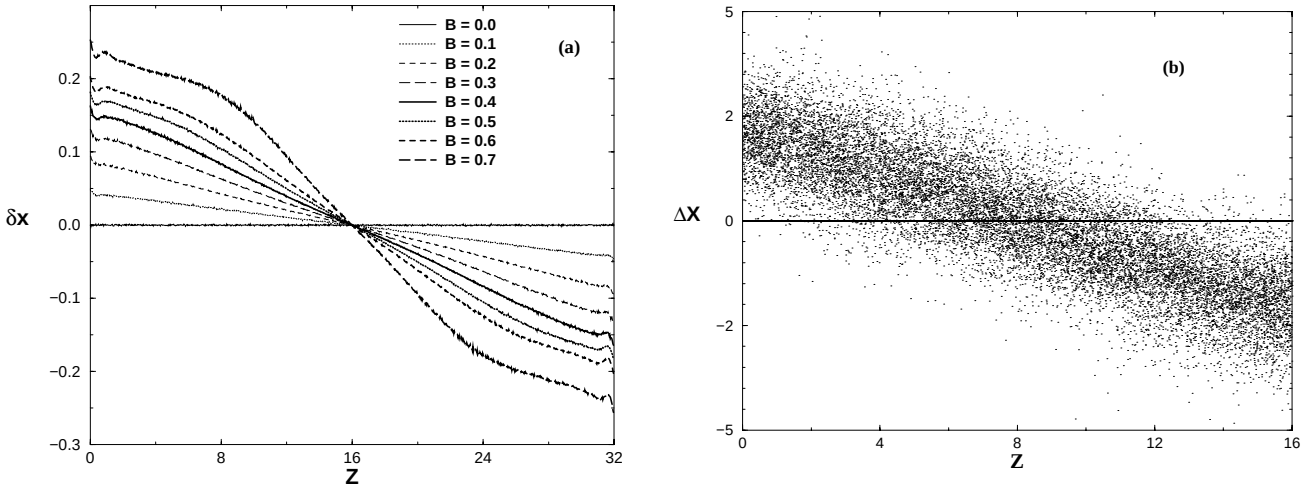

Fig. 2. (a) Variation of the average distance of *accepted* jumps in x-direction *vs.* z coordinate with the external field amplitude B in a box of size $Z_{\max} = 32$. (b) Variation of the average velocity (distance in x-direction traveled by a monomer after 1024 MCS) at density $c = 1.0$, $Z_{\max} = 16$, and $B = 0.1$.

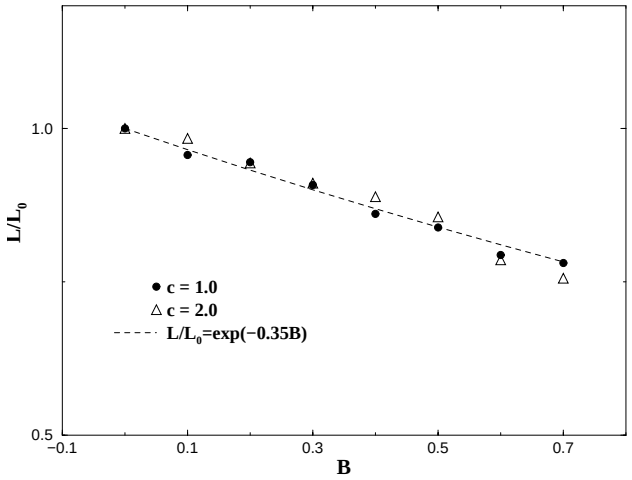

Fig. 3. Relative decrease of mean chain length L in lamellar flow field *versus* B at $J/kT = 7$, densities $c = 1.0$ and $c = 2.0$ and $D = 16$.

the derived values of L for $F \neq 0$ – the statistical error has been reduced at the expense of considerable computational effort. Note that the reduced L/L_0 mean chain length dependence on shear rate B (L_0 is the mean chain length of the solution at $B = 0$) appears to decrease nearly linearly with B: $L/L_0 = 1 - 0.35B$ which simply follows (*cf.* Eq. (10) below) from the exponential dependence of L on interaction J: $L/L_0 = \exp[-(J - bB)/2]/\exp(-J/2) = \exp(bB/2) \approx 1 - bB/2$ with the constant $b = 0.7$ measuring the effective decrease of bond energy J due to shear B. Another interesting observation is that the rate of decline is apparently independent of density c, at least for the small values of F considered in the present work.

The form for the MWD $C(l)$, that is, the concentrations of chains of contour length l, appears to change qualitatively for equilibrium polymers in dilute solutions. This change is in line with the predictions of the recent scaling theory of EP [4] where we demonstrated that the purely exponential form of the MWD, $P(x) \propto \exp(x)$, corresponding to concentration/chain length regimes in which density correlations are suppressed (typically beyond the semi-dilute threshold), is replaced by a "rounded" Schwartz power-exponential distribution:

$$P(x)\mathrm{d}x = \begin{cases} \exp(-x)\mathrm{d}x & (L \gg L^*) \\ \dfrac{\gamma^\gamma}{\Gamma(\gamma)} x^{\gamma-1} \exp(-\gamma x)\mathrm{d}x & (L \ll L^*) \end{cases} \tag{9}$$

when correlations are important (typically dilute concentrations). In equation (9) the reduced chain length, $x = l/L$, is taken as ratio of the particular chain length l to the mean chain length L, γ is the critical exponent of the $n \to 0$ vector model, (in 3D $\gamma \approx 1.165$ while its mean field value is $\gamma_{\mathrm{MFA}} = 1$), and L^* marks the average chain length at the crossover from dilute to semi-dilute concentration, ($c \to c^*$), of EP solutions. The mean chain length L was predicted and confirmed to vary with dimensionless bond energy $J/k_{\mathrm{B}}T$ as

$$L \propto c^\alpha \exp(\delta J/k_{\mathrm{B}}T) \tag{10}$$

with exponents $\alpha_{\mathrm{d}} = \delta_{\mathrm{d}} = 1/(1+\gamma) \approx 0.46$ in the dilute and $\alpha_{\mathrm{s}} = 1/2(1 + (\gamma - 1)/(\nu d - 1) \approx 0.6$, $\delta_{\mathrm{d}} = 1/2$ in the semi-dilute regime. In Figure 4 we plot $C(l)$ for a system at rest ($c = 0.5$, $B = 0$) and at maximum shear rate ($B = 0.7$) to demonstrate that the form of MWD changes qualitatively when shear is imposed. Thus it is evident from Figure 4 that in the presence of shear the correlations in polymer concentration in our dilute system of EP are effectively suppressed and the Molecular Weight Distribution is very well reproduced by the simple exponential function expected if a MFA description of the system holds. This finding can be understood if one recalls that the imposition of an external field with a shear rate B has a twofold effect on the polymers: (i) it effectively reduces the bond strength, $J \to J - bB$, which makes

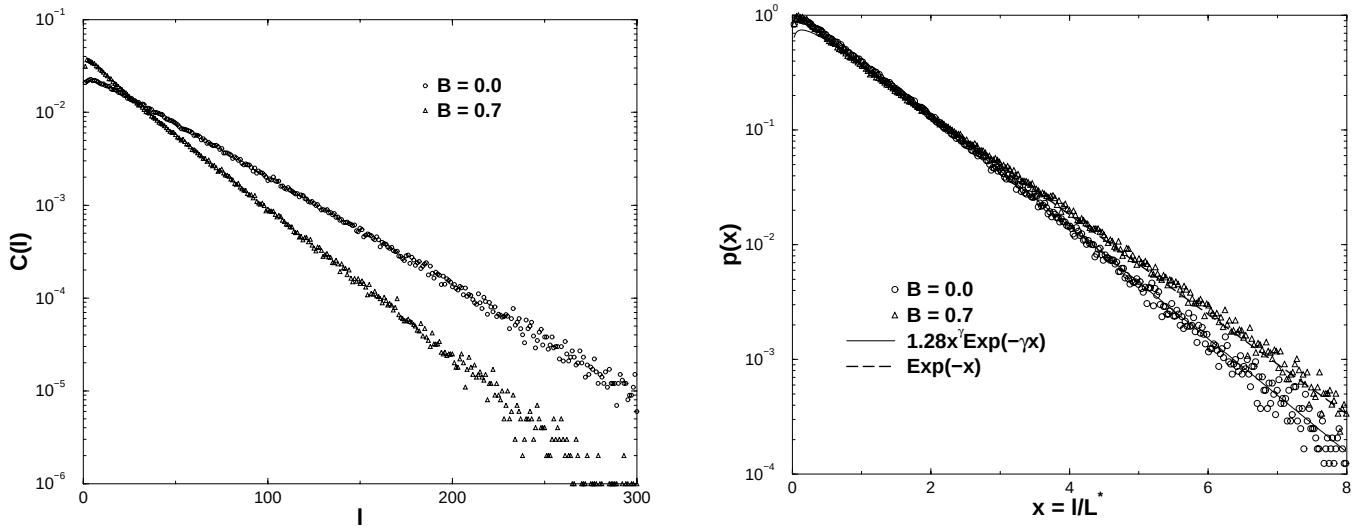

Fig. 4. (a) Molecular weight distribution in a system of EP at rest, $B = 0$, and in a flow, $B = 0.7$, at $J/kT = 7$ and monomer density $c = 0.5$. (b)The same as in (a) in dimensionless units $x = l/L$ fitted with equation (9) with $\gamma = 1.16$.

the polymers shorter, and (ii) the shape of the polymer coils is changed towards more rod-like shape with the longest axis oriented along the field. Meanwhile it is well known that a system of rods exhibits a Mean-Field-like behavior [2] which is here manifested by the change in the MWD – Figure 4.

3.3 Effect of shear rate on chain conformations

As the flow becomes faster, the individual shape of the chain coils change too. For weak shear rates B, the relative distortions (as measured for instance by flow birefringence [30]) are essentially proportional to τB where τ is the largest relaxation time of the unperturbed molecule [31]. Brownian dynamics studies [25] for Hookean dumbbells in a steady shear flow confirm this relative increase of the end-to-end distance with the shear rate both with and without hydrodynamic interactions included. A confirmation of these early predictions follows from our simulational results too – Figure 5.

In Figure 5 we plot the difference in gyration radii, typical for a large section of the length distribution and averaged over all EP, in two characteristic cases – system at rest and in a flow, indicating that chain coils in a flow become more extended along the field and compressed parallel to it. The result is a total increase of $R_{\rm g}^2$ as the whole system starts drifting along field's direction. It is also evident from Figure 5 that this asymmetry in the components of $R_{\rm g}^2$ becomes progressively more pronounced as l gets larger. The fact that $R_{{\rm g}z}^2$ is somewhat smaller than $R_{{\rm g}x}^2$ even at rest is due to the presence of hard walls at $z = 0, Z_{\max}$ which slightly deforms the coils in z-direction. We have not given here a plot of the z-dependence of $R_{\rm g}^2$ because of the surface segregation of

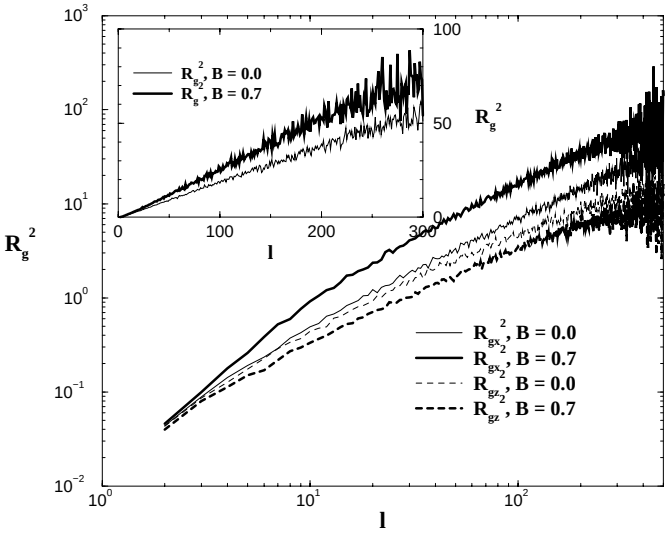

Fig. 5. Variation of coil size along the field, $R_{{\rm g}x}^2$, and perpendicular to field, $R_{{\rm g}z}^2$, with chain length l and two values of $B = 0.0,$ and 0.7. The inset shows the *total* $R_{\rm g}^2$ in normal coordinates. Here $J/kT = 7$ and the density $c = 0.5$ in a narrow slit $D = 16$. The average coil size measured at zero shear rate is $R_{\rm e}^2 = 50.03$ and $R_{\rm g}^2 = 8.325$.

chain lengths, induced by the parallel plates. This segregation populates the vicinity of the walls with single monomers and very short species. In contrast, the longer chains reside at least a distance $R_{\rm g}$ always from the walls (see next section). Such a distribution of centers of mass with respect to chain length takes place in EP even at rest (and is further enhanced by the flow) making the MWD

a z-dependent quantity and thus interfering with the pure effect of coil stretching under flow.

3.4 Density profiles

The overall transformations which the system undergoes with increasing shear rate, however, become much more explicit if density and diffusion profiles are sampled as function of z. This is shown in Figure 6 where the density is normalized to unity ($\int_0^D c(z)\mathrm{d}z = 1$). It is evident from Figure 6a that in the absence of bias when the system is at rest the total monomer density is uniformly distributed across the box with a typical depletion immediately at the walls (at low concentration of the solution). The walls are avoided by the longer chains because of entropic reasons. When the system starts to flow a redistribution of density sets in with increasing bias B whereby for the highest shear rate one observes a density maximum centered at the middle where the flow velocity is nearly zero. Qualitatively this density profile appears to be similar to analytic and simulational results [24] for the center of mass concentration profile between upper and lower walls, obtained earlier for a single dumbbell in a slit[3].

As the concentration is further increased, one observes the onset of typical oscillations in density profiles in the vicinity of the walls, Figures 6b and 6c. Such oscillations are typical for polymer solutions confined between flat plates and have been comprehensively studied for conventional polymers by Monte-Carlo simulations before [32,33]. The observed transitions in the monomer density immediately at the walls from a deficit (depletion layer) at low concentration up to an excess (for melts) are governed by a competition between entropic and packing effects. Because of the resultant decrease of configurational entropy it becomes unfavorable for polymers to be near the walls. Chains near the walls, on the other hand, suffer collisions with the chains away from the walls, and tend to move closer to the walls. At low density the entropic effect dominates, while at high densities packing effects prevail. This is clearly seen in Figures 6a, 6b and 6c for zero shear. In dilute solutions, as seen from Figure 6a, the increase of shear rate leads to effective broadening of the depletion layers, adjacent to the walls, which is in agreement with EWIF (evanescent wave-induced fluorescence) experimental observations [34] of GM, but at variance with an earlier computer simulation [26].

This density variation across the slit, caused by the shear rate, appears to depend essentially on the overall concentration of the system. At larger shear a density maximum still forms for the slowest layer of flow in the box middle at concentration $c = 1.0$ whereas for very dense systems, Figure 6c, this density redistribution with shear is suppressed. One may thus conclude that effects of shear on the density profiles in a slit depend essentially on the free volume in the system which is available for rearrangement of the polymer chains. In the broader slit, Figure 6d, where the shear rate gradually diminishes in the vicinity of the wall (adjacent layers flow with nearly equal velocity), the density profile gets more complex with two local minima and a sharp increase at the walls. This complex picture indicates that monomer density is generally increased in locations of zero flow or steady flow with vanishing shear.

Clearly, the changes in these profiles with B when shear sets on reflect some complex reorganization in the polydisperse system of EP whereby the "rapids" of the flow may act differently on chains of different length.

Additionally, even at rest, the system segregates in the vicinity of the walls for entropic reasons [11] into layers occupied predominantly by chains of decreasing contour length as one gets closer to the wall. These effects are indeed seen in Figure 7, where the average positions of the centers of mass of single monomers and of chains of length $l = 70$ are shown at various strengths of the bias field. The single monomers evidently tend to occupy the immediate vicinity of the walls and this tendency is enhanced as the shear increases. The long chains, on the contrary, keep at distance $\approx R_\mathrm{g}$ from the walls while the system is at rest. For growing B their residence is further narrowed around the "slow" region in the center of the box. In view of Figure 6a one may conclude that the deficit of single monomers from this region is more than compensated by accumulation of longer chains. In the wide slit ($D = 32$), only a fraction of the long chains still remains in the middle whereas two new maxima at the walls appear. Evidently, this happens in those regions where the shear rate for $B > 0.4$ (*cf.* Fig. 2) nearly vanishes.

One might expect that other properties of the system, related to density, will also be affected by the shear, as for instance, the local diffusion coefficient. In Figure 8 we plot a histogram of mean square displacements (MSQD), performed by all those particles which remain in the same z-layer within a MCS.

The distribution of MSQD, Figure 8, develops from being nearly constant (with two small wings at the depletion zones) for zero bias to a well defined broad minimum in the middle of the box as $B \to 0.7$ whereby as a whole it also decreases. Evidently, the diffusion profile across the channel reflects simply the variations of the density distribution.

3.5 Nematic ordering of short chains

Most of the simulational results, discussed in the preceding subsections, have been carried out for a sufficiently strong energy bond, $J/kT = 7$, which is equivalent to a rather low temperature of the system. The average chain length at $J/kT = 7$ thereby varies with density within the interval $40 \leq L \leq 70$ where the flexibility of the chains ensures that their conformations correspond to well shaped polymer coils. It is interesting to check whether a change in the mean size of the chains L in some way affects the reorganization of the polydisperse system under shear flow. If one reduces the ratio of bond to thermal energy $J/k_\mathrm{B}T$, as mentioned in the previous section, equation (10),

[3] In the much simpler model [24], however, the density profile is independent of the shear rate B.

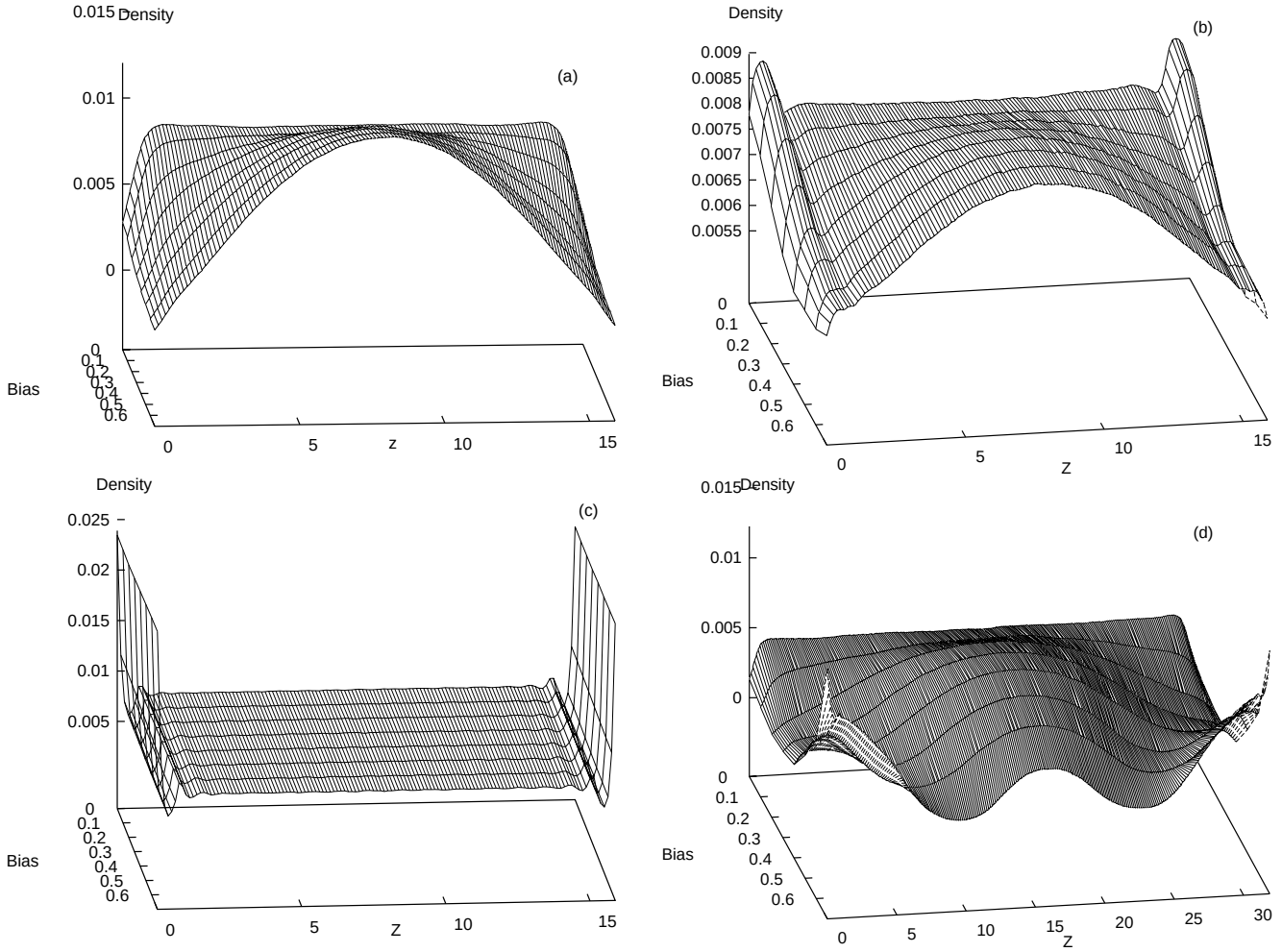

Fig. 6. Distribution of total monomer density between the hard walls in a slit of width $Z_{\max} = 16$ at varying shear rate (bias) and $J/kT = 7$: (a) $c = 0.5$; (b) $c = 1.0$; (c) $c = 2.0$; (d) a broad slit with $Z_{\max} = 32$ and $c = 0.5$.

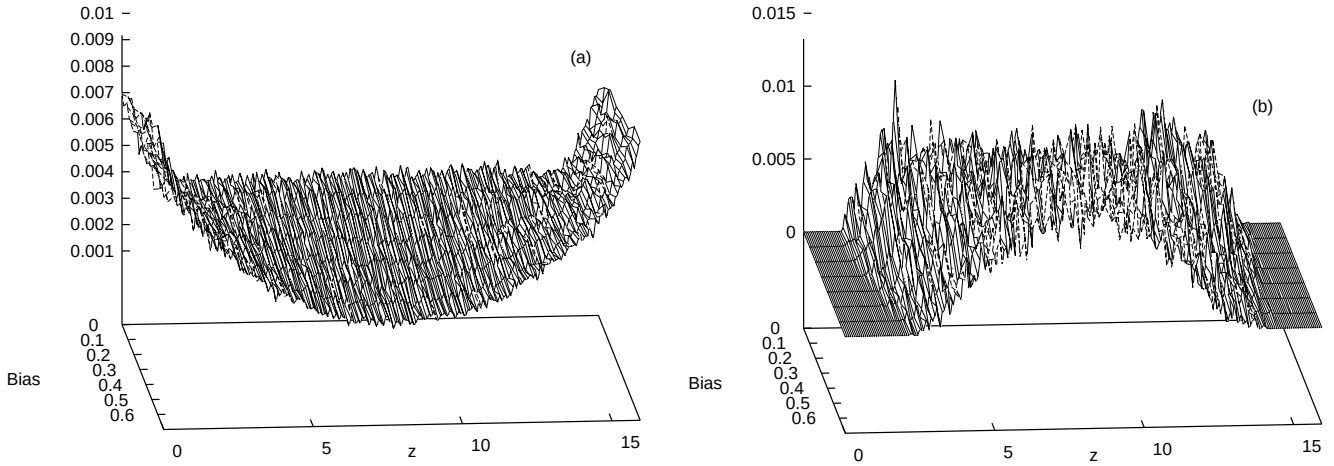

Fig. 7. (a) Center of mass distribution of single monomers in a slit with $D = 16$, $J/kT = 7$ and $c = 0.5$ at various values of the shear rate (bias). (b) Center of mass distribution of chains with $l = 70$ under the same conditions as in (a).

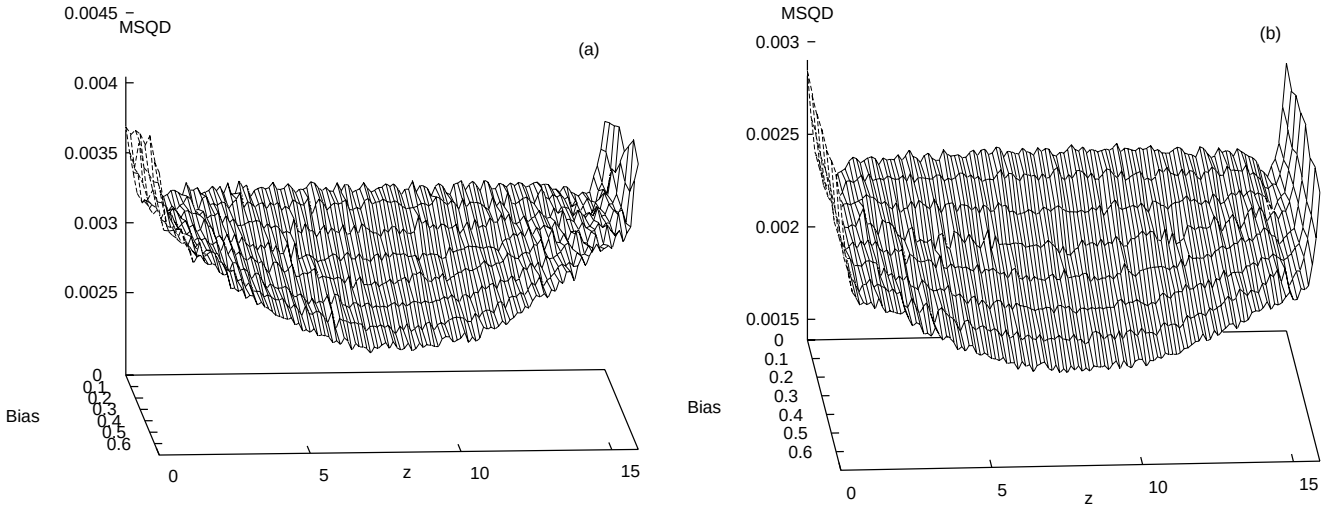

Fig. 8. Distribution of MSQD during 1 MCS in a box with $Z_{\max} = 16$ for different shear rates (bias) at $J/kT = 7$: (a) for $c = 0.5$; (b) for $c = 1.0$.

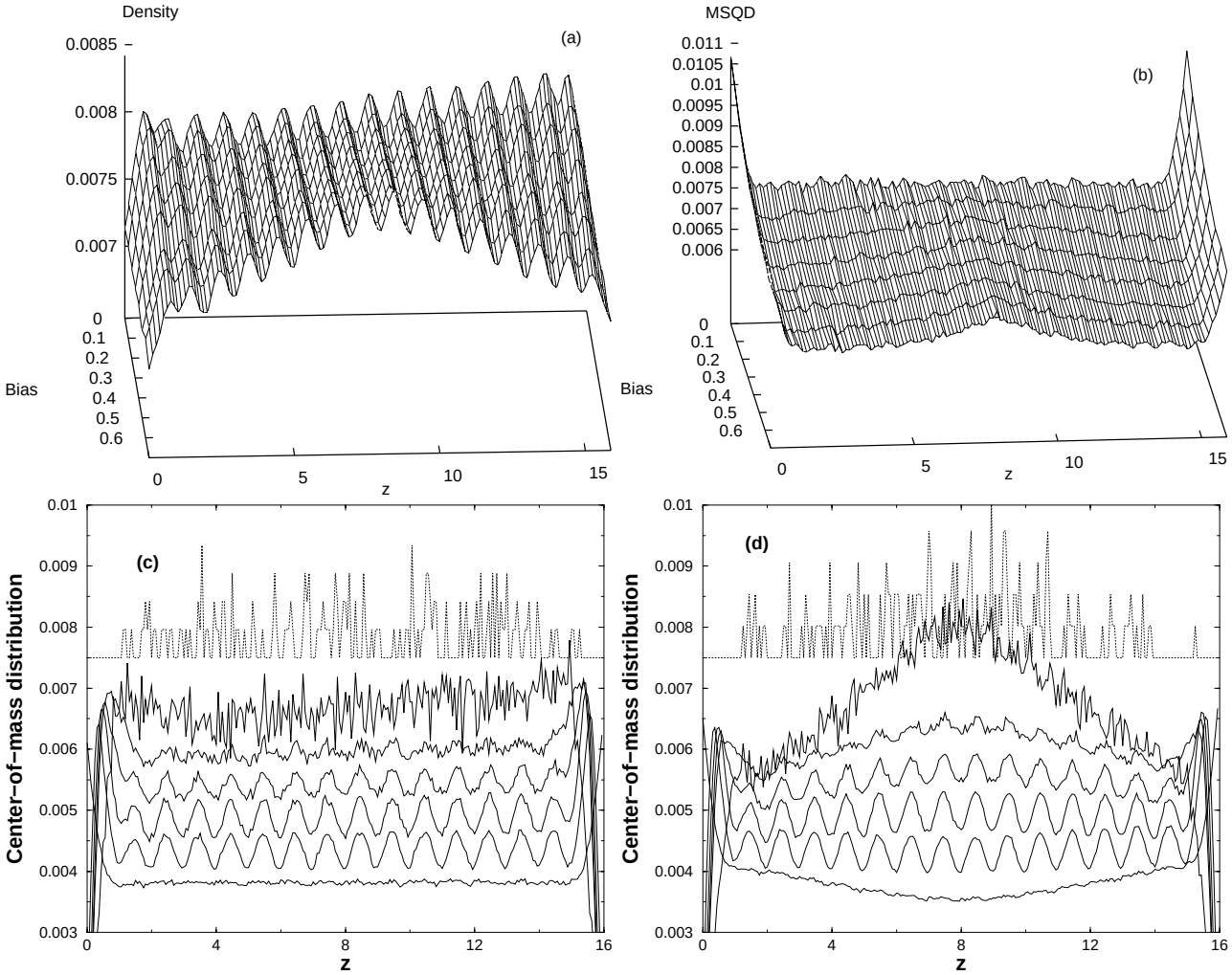

Fig. 9. (a) Distribution of the total monomer density across a slit with $D = 16$ at various rates of shear (bias). (b) Average mean square displacement after 1 MCS. (c) Center-of-mass distribution of chains with $l = 1, 2, 3, 4, 5, 10$ and 20 for $B = 0$. Each curve is shifted from the previous one along the y-axis at 0.0005 for better visibility. (d) The same as in (c) but for $B = 0.7$. The width of the slit is $Z_{\max} = 16$, $c = 0.5$ and $J/kT = 1$.

the average contour chain length decreases exponentially fast. In the present study we change J/kT from 7 down to 1 whereby L drops from ≈ 40 to 2.5. As shown below this leads to dramatic changes in the EP solution. The profiles along the z axis for this case of very short chains are shown in Figure 9.

The oscillations in the the total density, Figure 9, suggest a transition of the system into an ordered state of nematic liquid crystal with an easy direction parallel to the walls. Evidently the presence of hard walls acts as an external ordering field on the chains. The system is dominated by monomers, dimers and other very short species which behave largely like stiff rods aligning themselves parallel to the walls. Indeed, Figures 9c and 9d demonstrate that this ordering is most pronounced for dimers, trimers and tetramers whereas neither single monomers nor chains with length $l \geq 5$ participate in the ordering. Thus both single monomers, which lack any anisotropy in shape, and longer chains with conformations of coils rather than stiff rods are insensitive to the ordering influence of the walls.

The influence of growing shear rate on the system with $L = 2.5$ is similar to that in the case of $L \approx 40$ too. From Figures 9c and 9d one may conclude that the longer chains, which are otherwise uniformly distributed, now pull closer to the middle of the slit where the flow velocity is zero. This tendency starts with the 4- and 5-mers already and is very clearly seen for the 10-mers (there are only few 20-mers in the system at $J/k_{\rm B}T = 1$ and their statistics is therefore rather poor). This effect more than compensates the developing shallow minimum in single monomer concentration in the middle of the box.

4 Concluding remarks

The present simulational study of the impact of shear flow on EP in a slab reveals a number of interesting features:

- The average chain length in a system of EP decreases steadily with growing shear rate.
- The polymer coil is gradually stretched along the flow direction as the shear is increased.
- The MWD in a dilute solution of EP changes qualitatively when sufficiently strong shear rate is imposed from Schwartz- to a mean-field like exponential distribution function.
- The shear rate introduces inhomogeneity in the system of EP, confined in a slit: the monomer density, the diffusion coefficient and the concentration of macromolecules with different lengths develop characteristic profiles perpendicular to the walls.
- The width of the depletion layer near the wall for long chains grows with increasing shear rate in agreement with recent EWIF studies.

Another interesting phenomenon – an ordering transition in a system dominated by the shorter and stiffer chains is found to take place upon *heating* of the system of EP with the result that chain length is reduced. In this case shear flow is observed to enhance the degree of ordering in the system.

Our observations show that the relaxation of a system of EP from a state of rest to that of steady state flow is a slow process which requires long time intervals of investigation, probably rendering Monte-Carlo simulational methods probably more appropriate than Molecular Dynamics.

We should like to note, however, that the shear rates studied in the present work are limited to low and moderate values since stochastic jumps along and against the external field may be biased by means of the Boltzmann factor in a MC procedure within the framework of 100% at most. We therefore expect that at still higher shear rates the influence of flow on EP properties might be more dramatic. Clearly, additional work and adequate alternative methods are still needed to reach comprehensive understanding of the problem.

This research has been supported by the National Science Foundation, Grant No. INT-9304562 and No. DMR-9727714, and by the Bulgarian National Foundation for Science and Research under Grant No. X-644/1996. J.W. acknowledges support by EPSRC under Grant GR/K56233 and is indebted for hospitality in the Center for Simulational Physics at the University of Georgia.

References

1. A broad class of surfactants forming long flexible (wormlike) aggregates, called *giant micelles* (GM), consists of a polydisperse solution of differently long macromolecules which constantly recombine with each other, or break into smaller fractions [2]. In contrast to GM in *living polymers* (LP) equilibrium polymerization proceeds by means of a fixed amount of initiator, which activates one of the chain ends [3] so that single monomers may attach or break at the polymer end only. In many aspects the behavior of GM and LP in equilibrium is very similar, *e.g.* both are characterized by an exponential Molecular Weight Distribution (MWD).
2. M.E. Cates, S.J. Candau, J. Phys.-Cond. Matter. **2**, 6869 (1990).
3. S.C. Greer, Adv. Chem. Phys. **96**, 261 (1996).
4. J.P. Wittmer, A. Milchev, M.E. Cates, J. Chem. Phys. **109**, 834 (1998).
5. M. Kröger, R. Makhloufi, Phys. Rev. E **53**, 2531 (1996).
6. S.C. Greer, Comput. Mater. Sci. **4**, 334 (1995).
7. M.E. Cates, Of Micelles and Many-Layered Vesicles, in *Theoretical Challenges in the Dynamics of Complex Fluids*, edited by T. McLeish, NATO ASI Series, pp. 257-283.
8. A. Milchev, J. Wittmer, D.P. Landau, (submitted for publication).
9. A. Milchev, Y. Rouault, D.P. Landau, Phys. Rev. E **56**, 1946 (1997).
10. A. Milchev, Polymer **34**, 362 (1993).
11. A. Milchev, D.P. Landau, J. Chem. Phys. E **104**, 9161 (1997).
12. J.F. Berret, D.C. Roux, G. Porte, P. Lindner, Europhys. Lett. **25**, 521 (1994).

13. V. Schmitt, F. Lequeux, A. Pousse, D. Roux, Langmuir, **10**, 955 (1994).
14. R. Makhloufi, J.P. Decruppe, A. Ait-Ali, R. Cressely, Europhys. Lett. **32**, 253 (1995).
15. I. Furo, B. Halle, Phys. Rev. E **51**, 466 (1995).
16. S.Q. Wang, W.M. Gelbart, A. Ben-Shaul, J. Phys. Chem. **94**, 2219 (1990).
17. S.Q. Wang, Macromolecules **24**, 3004 (1991).
18. N.A. Spenley, M.E. Cates, T.C. McLeish, Phys. Rev. Lett. **71**, 939 (1993).
19. F. Rondelez, D. Ausserre, H. Hervet, Annu. Rev. Phys. Chem. **38**, 3056 (1987).
20. P.G. de Gennes, J. Chem. Phys. **60**, 5030 (1974).
21. J.H. Aubert, M. Tirrell, J. Chem. Phys. **72**, 2694 (1980).
22. A. Onuki, J. Phys. Soc. Jap. **54**, 3656 (1985); A. Onuki, Phys. Rev. Lett. **62**, 2472 (1989).
23. P. Biller, F. Petruccione, J. Non-Newtonian Fluid Mech. **25**, 347 (1987).
24. C.J. Goh, J.D. Atkinson, N. Phan-Thien, J. Chem. Phys. **82**, 988 (1984).
25. F.G. Diaz, J. Garcia de la Torre, J.J. Freire, Polymer **30**, 259 (1989).
26. E. Duering, Y. Rabin, Macromolecules **23**, 2232 (1990).
27. J. Wittmer, W. Paul, K. Binder, Macromolecules **25**, 7211 (1992).
28. I. Gerroff, A. Milchev, W. Paul, K. Binder, J. Phys. Chem. **98**, 6526 (1993).
29. A. Milchev, W. Paul, K. Binder, J. Phys. Chem. **99**, 4786 (1993).
30. J. Kriegl, Adv. Polymer Sci. **6**, 170 (1969).
31. B.H. Zimm, J. Chem. Phys. **24**, 269 (1956).
32. A. Yethiraj, C.K. Hall, Macromolecules **23**, 1865 (1990).
33. R. Pandey, A. Milchev, K. Binder, Macromolecules **30**, 1194 (1997).
34. D. Aussere, J. Edwards, J. Lecourtier, H. Hervet, F. Rondelez, Europhys. Lett. **14**, 33 (1991).